

THE EFFECT OF GAMMA-PRIME PHASE DISTRIBUTION ON ELEVATED TEMPERATURE TENSILE PROPERTIES IN A SINGLE CRYSTAL SUPERALLOY.

M.B.Henderson\* and J.W.Martin.\*

ABSTRACT. Two types of  $\gamma'$ -phase distribution in SRR 99 single crystals have been studied, one produced by the standard heat-treatment containing aligned cuboids along  $\langle 100 \rangle$ , and one with coarse rods of  $\gamma'$ . Tensile properties have been compared at room temperature, 650°C and 850°C, and the fracture mode studied metallographically. The shapes of the stress-strain curves, and the fracture modes are temperature dependent. The standard aged material exhibits the optimum in tensile properties at 20°C and 650°C, whilst at 850°C the flow behaviour of the two structures is comparable. Interconnected rods of  $\gamma'$  appear to deflect  $\{100\}$  propagating cracks, and this structure shows enhanced ductility.

INTRODUCTION

SRR 99 is a nickel-based single crystal superalloy developed for use in turbine blade applications. Previous work (1) has shown that the size, shape and distribution of the  $\gamma'$  phase in SRR 99 can be altered by varying the ageing treatment of the alloy. The standard heat-treatment produces a cuboidal array of  $\gamma'$  particles aligned along  $\langle 100 \rangle$ . It has been shown that under fatigue conditions (2, 3), at elevated temperatures, crack growth takes place through the  $\gamma$  matrix along a 'soft'  $\{100\}$  propagation path, and also (4) creep cracks propagate (at 750°C) along  $\langle 100 \rangle$ .

The present work explores the effect of changing the  $\gamma'$  distribution to an array of interconnected rods upon the elevated temperature tensile properties. It was hoped that such an array would interrupt  $\langle 100 \rangle$  cracks in the  $\gamma$  matrix, and thereby enhance the intrinsic toughness of the microstructure. This forms part of an ongoing research investigation into the high temperature fatigue and tensile properties of SRR 99.

EXPERIMENTAL

The nominal composition of SRR 99 is given in Table 1.

\* Oxford University Department of Materials, UK.

TABLE 1 Composition of SRR 99(wt %)

Al	Ti	Cr	Co	Ta	W	C	Ni
5.5	2.2	8.5	5.0	2.8	9.5	0.015	Bal.

After solution treatment for 4 hours at 1300°C, specimens were aged as follows:

A. Standard ageing consisting of 1 hour at 1100°C then 16 hours at 870°C, resulting in regular cuboidal arrays of  $\gamma'$  aligned along  $\langle 100 \rangle$  in the  $\gamma$  matrix (fig.1).

B. Ageing for 72 hours at 1100°C followed by 16 hours at 870°C producing an array of aligned  $\gamma'$  rods, together with a dispersion of fine  $\gamma'$  particles (fig.2).

Tensile tests on  $\langle 100 \rangle$  oriented cylindrical specimens with these microstructures have been conducted at 20°C, 650°C and 850°C at a strain rate of  $4 \times 10^{-4} \text{ s}^{-1}$ .

The fracture surfaces have been studied using SEM, and longitudinal sections of the fractured gauge lengths have also been examined.

#### EXPERIMENTAL RESULTS AND DISCUSSION

##### Tensile Tests.

Figs.3 and 4 show the stress-strain curves obtained for specimens having microstructures A and B above, at 20°C, 650°C and 850°C. The 20°C curves exhibit little work-hardening, whereas at 650°C conventional three-stage work-hardening characteristic of an f.c.c. single crystal is discernable. At 850°C monotonic curves are observed.

In the case of A, (fig.3) high room temperature strength is maintained to 650°C, but at 850°C the flow stress is reduced and the strain to fracture is increased. This pattern of behaviour can be explained by an increase in the strength of the  $\gamma'$  with increasing temperature (5), whereas that of the matrix decreases.

The yield stresses and elongations obtained by averaging the results of several tests are summarized in Table 2, although a better comparison is obtained from the entire curves. At room temperature and 650°C B is weaker than A, but at 850°C B exhibits an improved ductility with little loss in strength. A comparison of the curves for A and B at 850°C indicates that their flow stresses are in fact comparable.

TABLE 2. Tensile test data.

	Temperature/°C	Yield Stress/MPa	% Elongation
A	20	1107	8.8
	650	1087	8.4
	850	968	14.7
B	20	788	21.3
	650	883	13.6
	850	888	18.5

Tensile fractography.

20°C. The deformation mode was highly planar. Fracture occurred at the gauge-length shoulder macroscopically perpendicular to the tensile axis. Fig.5 shows the fracture surface of structure B, where intersecting {111} traces are in evidence. Final fracture was by microvoid coalescence associated with the  $\gamma'$  precipitates.

650°C. Fracture occurred in both microstructures on a single {111} plane in the middle of the gauge length, with evidence of fine scale local plasticity (fig.6). Intense surface slip bands were also apparent, both primary (lying parallel to the final fracture plane) and secondary in character. This suggests that  $\gamma'$  shearing is occurring leading to highly planar plastic deformation and final failure on a single plane of shear.

850°C. All specimens necked and fractured on a plane roughly perpendicular to the tensile axis, which suggests a much more homogeneous deformation mode. The important role of the interdendritic porosity in the nucleation of the final fracture is evident in fig.7(a,b) where {100} planar cracks emanating from the pores interlinked by {111} shear planes can be seen. In B (fig.7b) the interlinking final shear process has led to a much rougher surface, whose scale reflects the coarser  $\gamma'$  distribution.

Longitudinal sectioning showed that internal cracks form by microvoid coalescence. These occur at interdendritic regions where, in the absence of grain boundaries, brittle phases and eutectic regions are apparent along with a large number of {100} cracks formed at shrinkage pores. They interlink by means of intense {111} shear (fig.8). Examination of the {100} cracks in structure B indicates that there is some tendency for the propagating cracks to follow the matrix and avoid cutting the  $\gamma'$  rods. This will increase the work of fracture, although it is apparent that some degree of precipitate cutting occurs.

CONCLUSIONS

1. Conventionally heat-treated SRR 99 appears to exhibit optimum tensile properties at room temperature and 650°C.

2. At temperatures up to 650°C slip is essentially heterogeneous, whilst at 850°C it is more homogeneous, due to the change in dislocation/ $\gamma'$  particle interaction.
3. At 850°C void and microcrack formation play a crucial part in the eventual failure of this material. Fracture is initiated at crystal imperfections arising from the casting process.
4. At 850°C the two structures have similar stress-strain curves, with structure B showing the greater ductility.
5. Crack meandering would appear to be enhanced by the rod-like  $\gamma'$  morphology.

#### ACKNOWLEDGEMENTS

The authors are grateful to the SERC and to the Procurement Executive of the Ministry of Defence for support, and to Professor Sir P.B. Hirsch, FRS for the laboratory facilities made available.

#### REFERENCES

1. Hopgood, A.A. and Martin, J.W. (1986) 'The coarsening of  $\gamma'$  precipitates in a single crystal superalloy', *Materials Science and Technology* 2, 543-
2. Crompton, J.S. and Martin, J.W., (1984) *Trans. AIME* 15A: 1711.
3. Murphy, O.R. and Martin, J.W. (1988) 'Fatigue crack propagation in a single crystal superalloy at elevated temperature' *Proc. 7th European Conf. on fracture, Budapest*, 1138-
4. Hopgood, A.A. and Martin, J.W. (1986) 'The creep behaviour of a nickel-based single crystal superalloy'. *Materials Science and Engineering* 82, 27-36.
5. Copley, S.M. and Kear, B.H. (1967) *Trans. Met. Soc. AIME* 239, 977.

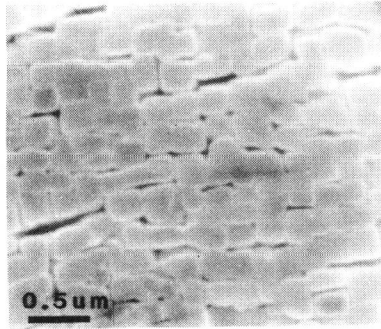


Fig.1 SEM micrograph of SRR 99 after Treatment A.

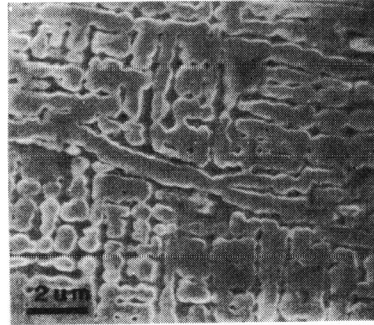


Fig.2 SEM micrograph of SRR 99 after Treatment B.

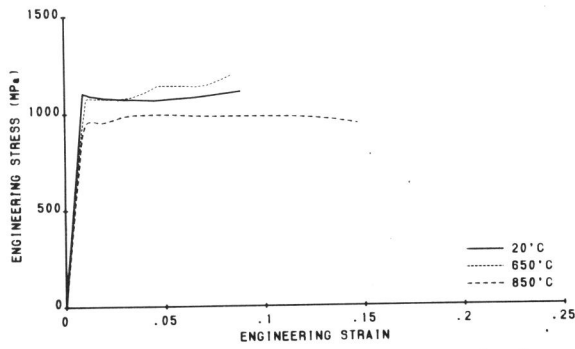


Fig.3 Stress-strain curves for SRR 99 having Microstructure A.

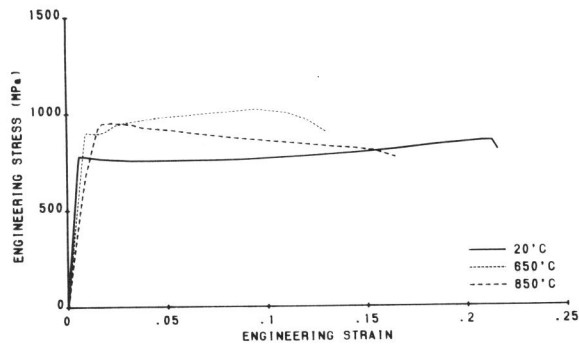


Fig.4 Stress-strain curves for SRR 99 having Microstructure B.

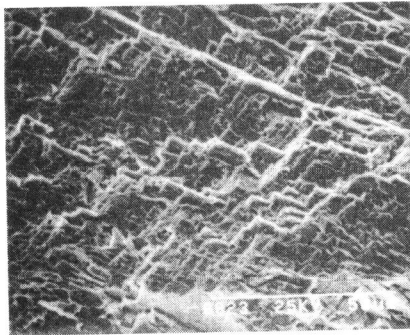


Fig.5 SEM micrograph: 20°C tensile fracture in structure B.

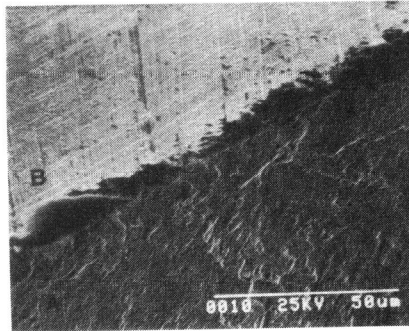
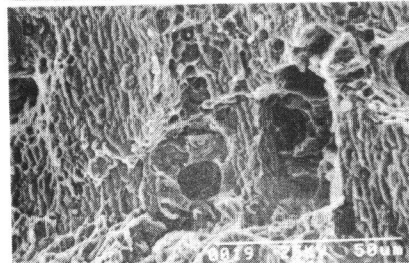
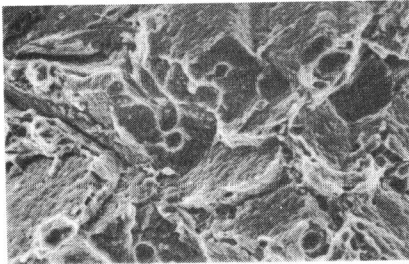


Fig.6 SEM micrograph: 650°C tensile fracture in structure A; fracture surface is at region A; surface slip bands at region B.



Figs.7(a,b) SEM micrographs: 850°C tensile fractures in structures A and B respectively.

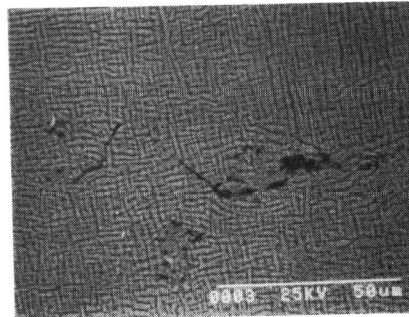


Fig.8 Interconnecting {111} shear between microcracks formed at 850°C in structure B (SEM micrograph).